**Supplemental Materials for: Feasibility Studies of a New Event Selection Method to Improve Spatial Resolution of Compton Imaging for Medical Applications**

## APPENDIX A. DCA CALCULATION

The DCA is calculated using the following method. For each incident $\gamma$ emitted from a known source position, the scattering angle is calculated, and the apex of the back-projected cone-of-origin is determined. The apex of the cone is equal to the first interaction location ($P_1$), the axis of the cone is found using the vector between the first two interaction points in the detector, and the scattering angle (opening angle of the cone) is calculated using (3), as shown in Fig. 10.

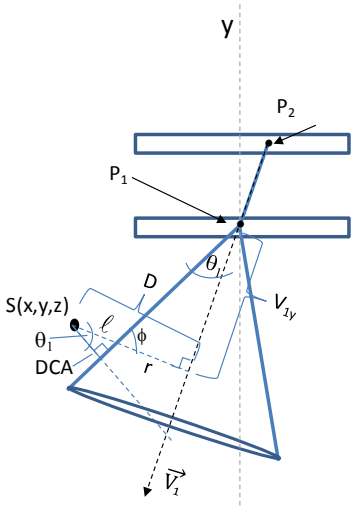


Figure 10: Calculation of the distance of closest approach (black line) between the origin cone and the actual position of the point source.

The perpendicular distance (D) between the source position (S) and the cone axis is determined using the magnitude of the perpendicular vector from S to the cone axis. The radius of the cone ($r$) is determined using the y-coordinate of the source in the reference frame of the cone axis ($V_{1y}$)

$$r = V_{1y} \tan\theta_1. \tag{13}$$

Finally, DCA is calculated as the perpendicular distance from S to the cone surface, and is determined using

$$DCA = \ell \cos\theta_1 \tag{14}$$

where $\ell = D - r$. This value of DCA is calculated for each measured $\gamma$ and used to determine its initial energy and whether the $\gamma$ is acceptable for use in image reconstruction as described in section IV.A.

For extended line sources, the derivation of DCA changes because, rather than knowing the exact location of the point of $\gamma$ emission, we know only the central axis of the source. To find the distance of closest approach between the $\gamma$ cone-of-origin and the source central axis, the first thing that must be determined is the tilt angle between the cone surface and the y-axis. This is determined using the first two interaction vertices ($(x_1, y_1, z_1)$ and $(x_2, y_2, z_2)$ respectively) and the scattering angle from the first interaction ($\theta_1$). Then, from Fig. 10(a)

$$\begin{aligned} d &= \sqrt{(x_2 - x_1)^2 + (z_2 - z_1)^2} \\ h &= \sqrt{(x_2 - x_1)^2 + (y_2 - y_1)^2 + (z_2 - z_1)^2} \\ f &= \cos^{-1}\left(\frac{y_2 - y_1}{h}\right) \\ a &= f - q \end{aligned} \tag{15}$$

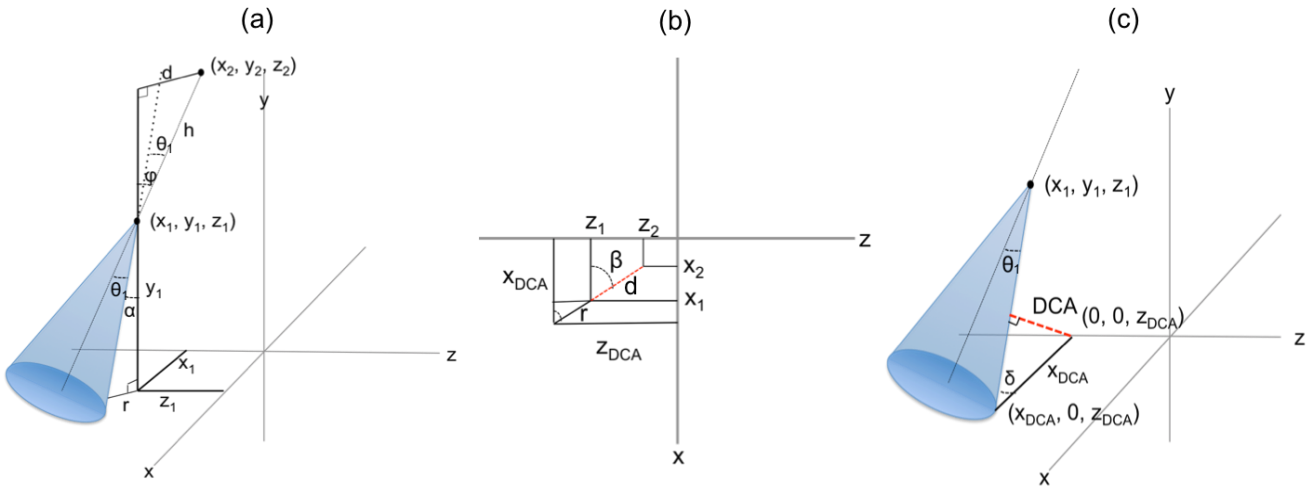


Figure 11: Schematic showing the calculation of the DCA for proton beam data. (a) shows the initial interaction positions and the back-projected cone-of-origin, as well as the tilt angle. (b) shows the parameters for calculating the distances to the surface of the cone in the x-z plane. (c) shows the final calculation of the DCA.

Next, the distance from the cone surface to the $y_1$-axis ($r$) can be determined, along with the angle between $r$ and the z-axis

$$r = y_1 \tan a$$
$$b = \tan^{-1}\left(\frac{z_1 - z_2}{x_1 - x_2}\right) \tag{16}$$

In order to determine DCA, the distance from the x and z-axes to the cone surface must be calculated ($x_{DCA}$ and $z_{DCA}$), as well as the angle between the cone surface and the x-z plane (δ). From Figure 10(b) these values are

$$x_{DCA} = \left(r + d + \sqrt{x_2^2 + z_2^2}\right)\cos b$$
$$z_{DCA} = \left(r + d + \sqrt{x_2^2 + z_2^2}\right)\sin b \tag{17}$$

while δ is determined using the cross product between $v_a = (x_1 - x_{DCA}, y_1, z_1 - z_{DCA})$ and $v_b = (-x_{DCA}, 0, 0)$, see Figure 10(c), giving

$$\delta = \cos^{-1}\left(\frac{v_a \cdot v_b}{|v_a||v_b|}\right)$$
$$= \cos^{-1}\frac{(x_1 - x_{DCA})(-x_{DCA})}{x_{DCA}\sqrt{(x_1 - x_{DCA})^2 + y_1^2 + (z_1 - z_{DCA})^2}}. \tag{18}$$

Finally, the DCA can be calculated using

$$DCA = x_{DCA}\sin d. \tag{19}$$

This value of DCA is calculated for each measured $\gamma$ and then used to determine its initial energy and for event filtering.

## APPENDIX B. POINT SOURCE MEASUREMENTS

*B1. Single point source efficiency.* For the $^{60}$Co measurements, data was collected in single-stage mode for 108,900 seconds. For the initial source activity of 0.66 $\mu$C this equated to 2.65 x $10^9$ gammas (1.17 MeV and 1.33 MeV) emitted. During the measurement a total of 1.22 x $10^6$ double/triple scatters were detected giving a raw double/triple detection efficiency of 4.6 x$10^{-4}$. This is a factor of ~20 higher than reported by [23] for the Polaris J CC, but this is to be expected since they measured data in multi-stage detection mode. Similarly, raw efficiency values of 1.9 x $10^{-4}$ per emitted gamma and 7.6 x $10^{-4}$ per emitted gamma were calculated for the $^{137}$Cs and $^{22}$Na (511 keV and 1.227 MeV) sources, respectively.

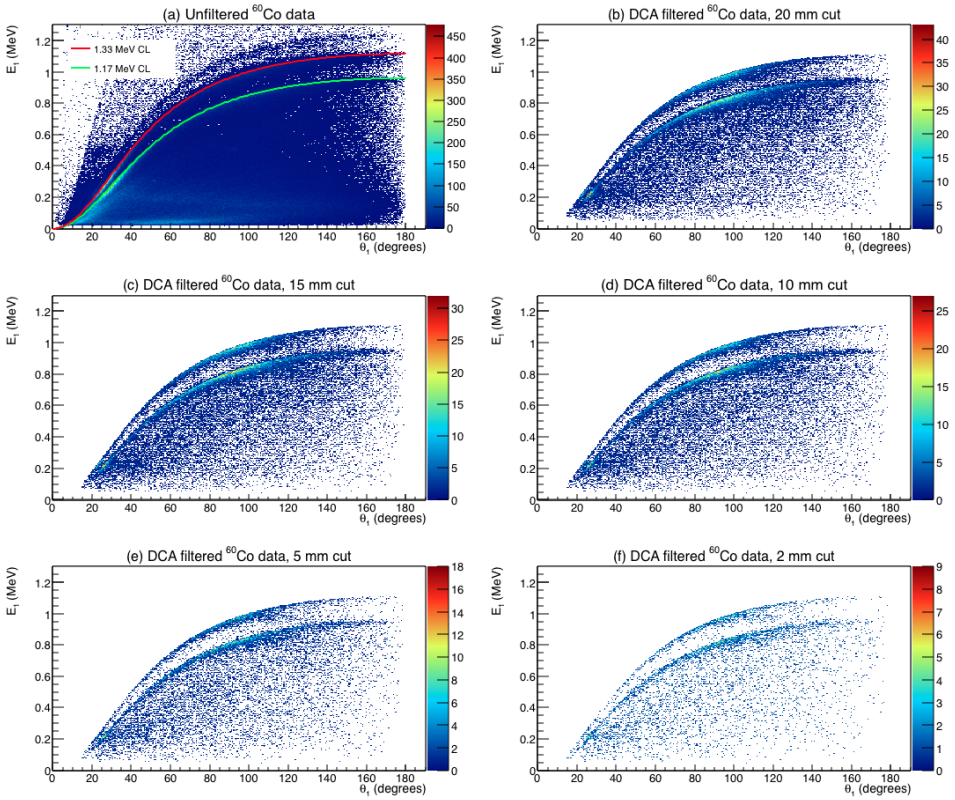


Figure 12: Measured $E_1$ values vs calculated $\theta_1$ for (a) unfiltered $^{60}$Co data and the same data after DCA filters of (b) 20 mm, (c) 15 mm, (d) 10 mm, (e) 5 mm, and (f) 2 mm were applied. The final number of scatter events used for reconstruction was 368,321 for the unfiltered data, and 87,973, and 69,200, 48,616, 25,708, and 10,391 for the data with DCA = 20 mm, 15 mm, 10 mm, 5, mm, 2 mm, respectively.

*B2. DCA and CL filter limits.* Fig. 12 shows the effect of DCA filter limits on the data used for reconstruction. As the DCA filter size was decreased, the number of events used for reconstruction decreased from 87,973 for DCA = 20 mm down to 10,391 for DCA = 2mm. As the number of events accepted by the DCA filter decreased, many of the events correlated to the CLs remain in the data while those events below and not along the CLs are removed from the data. As a result, the final image initially improves as the number of "good scatter" events along the CLs becomes a greater percentage of the total number of events. However, as can be seen in Fig. 13, as the DCA filter continues to decrease the number of events remaining falls to a point where statistical noise in the final image begins to increase acting to reduce the quality of the final image. Therefore to balance the reduction of noise due to "bad" events not correlated to the CLs and increase in statistical noise due to a low number of events used for the reconstruction, we chose DCA = 5 mm for our further point source studies.

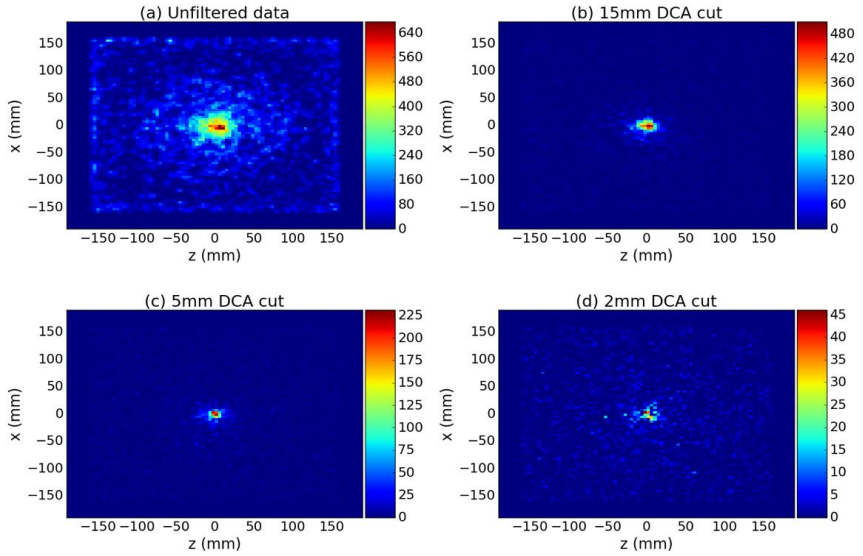


Figure 13: 2D projection images of the $^{60}$Co point source with (a) unfiltered data, and filtered with (b) DCA = 15 mm, (c) 5 mm, and (d) 2 mm.

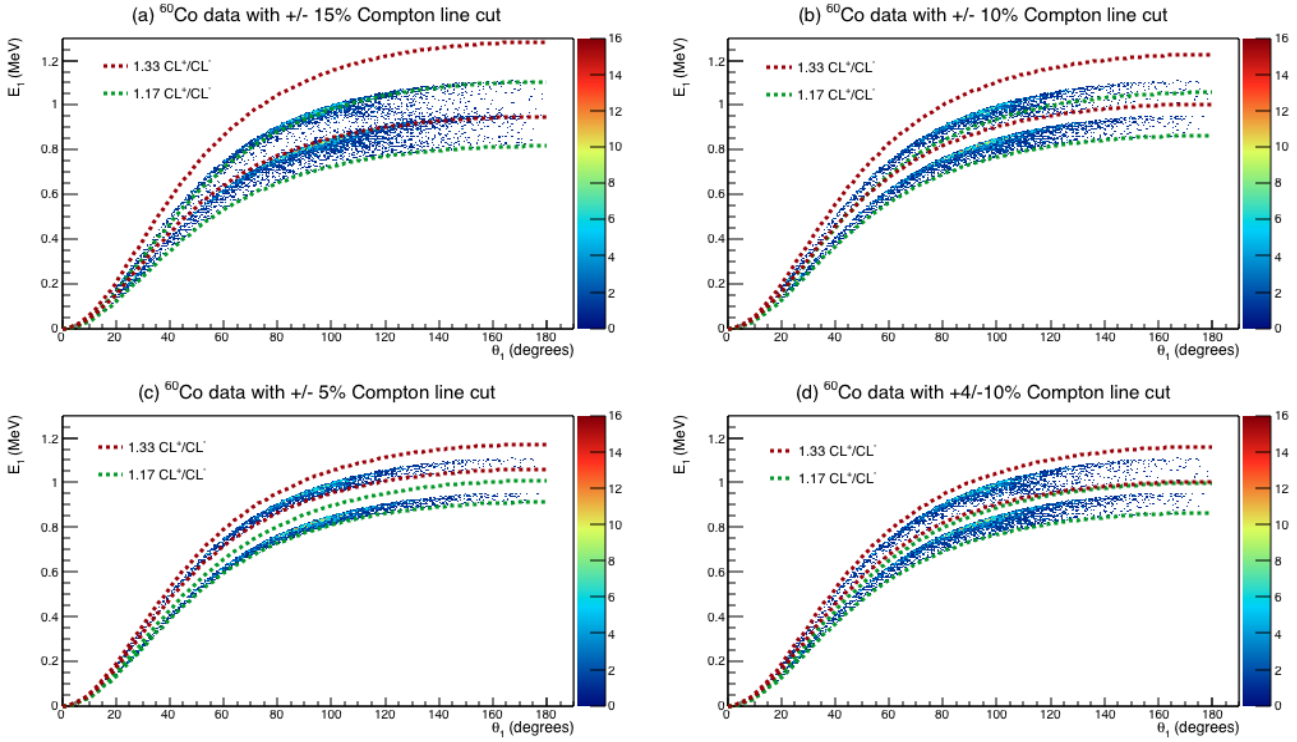


Figure 14: Measured E1 values vs calculated $\theta_1$ for the Compton Line filtered 60Co data after DCA filtering (DCA = 5 mm) for CL values of (a) ± 15%, (b) ± 10% (c) ± 5%, and (d) +4%/-10%.

For the CL filter, as shown in Fig. 14, as the limits of the filter decrease the number of events selected by the filter also decreases. For the data (post filtering with DCA = 5 mm) when a ±15% CL filtered data is applied the number of usable events drops to 8619 events and declines further to 7627, 4303 as the CL filter is reduced to ±10%, and ±5% respectively. Similar to the DCA filter results, as the CL filter becomes too restrictive, too few events will remain in the data to produce a usable image of the source. Therefore, as a compromise between reducing noise due to "bad" scatter events and still having adequate number of events to produce a usable image, we chose a CL = +4%/-10%, giving 6203 events for the $^{60}$Co source for this feasibility study.

## APPENDIX B. GLOSSARY OF TERMS

$\boldsymbol{CL^+}$ Upper limit for Compton line filter, expressed in percentage above theoretical acceptable $E_1$ value. (Equation 8a, Section IV.B)

$\boldsymbol{CL^-}$ Lower limit for Compton line filter, expressed in percentage below theoretical acceptable $E_1$ value. (Equation 8b, Section IV.B)

**D2C** Name of our imaging method. Stands for **D**CA + **C**L **C**ompton imaging method. (Sections I and IV)

**DCA** Distance-of-closest approach of the $\gamma$ cone-of-origin to the known source position (see Appendix A for derivation). Refers to the DCA Energy Determination method of determining $E_0$ of a $\gamma$ and using the determined "DCA-filter" to remove bad events. (Equation 4, Section IV.A)

$\boldsymbol{DCA(E_i)}$ The DCA value for a given initial guess at the initial $\gamma$ energy $E_i$. (Equation 6, Section IV.A.1)

**DCA filter** The maximum value the DCA is allowed to have before the event is rejected. (Section IV.A.2)

$\boldsymbol{\Delta E_i}$ The energy increment in which $E_i$ is adjusted as it is scanned over a defined energy range to determine $E_0$ of the $\gamma$ with the DCA Energy Determination process. (Section IV.A.1)

$\mathbf{E_0}$ The initial energy of the incident $\gamma$ determined from the energy deposited in the detector stages (i.e. $E_1$ and $E_2$). (Equations 1 and 2, Section I)

$\boldsymbol{E_0^{DCA}}$ DCA determined initial $\gamma$ energy. (Equations 9 and 10, Sections IV.A.1, IV.A.2, and IV.C)

$\mathbf{E_1}$ The energy deposited in the first interaction in the detector. (Equations 1 and 2, Section I)

$\mathbf{E_2}$ The energy deposited in the second interaction in the detector. (Equations 1 and 2, Section I)

$\boldsymbol{E_i}$ Initial guess at the initial $\gamma$ energy when performing DCA Energy Determination. $E_i$ is scanned over a range of energies in increments of $\Delta E_i$ to determine the initial $\gamma$ energy if $E_0$ is unknown. If the $\gamma$ is from a source with known emission lines (as in the case of $^{60}$Co or other point sources), then these emission line values are chosen as $E_i$. (Equation 6, Section IV.A.1)

$\boldsymbol{\ell}$ The distance from the point source to the surface of the cone-of-origin, perpendicular to the cone axis. (Equations 6 and 14, Section IV.A.1, Appendix A)

$\boldsymbol{r}$ Radius of the cone-of-origin. (Equations 13 and 16, Section IV.A.1, Appendix A)

$\boldsymbol{\theta_1}$ Scattering angle between the first two interactions, determined by the initial incident $\gamma$ energy ($E_0$) and $E_1$. (Equation 3, Section I)

$\boldsymbol{\theta_2}$ Scattering angle between the second and third interaction, determined using the vector between the first and second interactions ($v_1$) and the vector between the second and third interactions ($v_2$). (Equation 2, Section I)

$\boldsymbol{V_{1y}}$ Y-coordinate of the source along the cone axis. Used to compute the cone-of-origin radius. (Appendix A)